

Human/Robot Interaction via the Transfer of Power and Information Signals Part II: An Experimental Analysis

H. Kazerooni

Mechanical Engineering Department, University of Minnesota
111 Church Street SE, Minneapolis, MN 55455

Abstract

The work presented here is focused on the issues related to the dynamics and control in human/machine interaction in the sense of transfer of power and information signals. In Part I, the extender is defined as an active manipulator worn by a human to increase the "strength" of the human wearing it. The human body, in physical contact with the extender, exchanges information signals and power with the extender. The dynamic model of the extender system consists of three main parts: the human arm, the extender, and the environment. A single-degree-of-freedom hydraulic extender has been designed and built for experimental verification of the stability and performance criteria. An expression for the system performance has been derived as a means to describe the force augmentation of the system. The stability and performance of the extender is shown via simulation and experiments. The trade-off between the performance and stability is discussed, it is shown the more performance (larger force amplification) is required, the narrower stability range will be.

1. Introduction

To understand the issues in control and dynamics involved in human/machine interaction via the transfer of power and information signals, an experimental one-degree-of-freedom extender is described here. The general building blocks on nonlinear dynamics and control (in particular, the stability of the human and extender taken as a whole) are given in Part I of this paper. Figure 1 shows the schematic of the one-degree-of-freedom experimental prototype extender in maneuvering a load. Two forces add up to maneuver the extender: f_{eh} and τ . The contact force between the human and the extender, f_{eh} , is the result of human intention to move up the extender, and the actuator torque, τ , is the result of the feedback. A velocity controller is chosen as the primary controller for the extender so that the extender is stabilized independently of the human dynamic behavior¹.

When the human pushes against the extender, the contact force, f_{eh} , is measured and passed through the compensator, H_1 . The output of this compensator is used as the input command for the primary controller of the extender. Compensator H_2 is also chosen to generate compliance [14] in the extender in response to the forces imposed on the extender end-point. When the human does not push against the extender, the contact force, f_{eh} , and, consequently, the input command to the primary controller are zero.

¹ It is of practical importance that the extender be stable when the human is not wearing it. One can use a variety of control methods in the development of velocity controller for the extender. Reference 24 describes a method of tracking method for nonlinear systems. All references are listed in Part I.

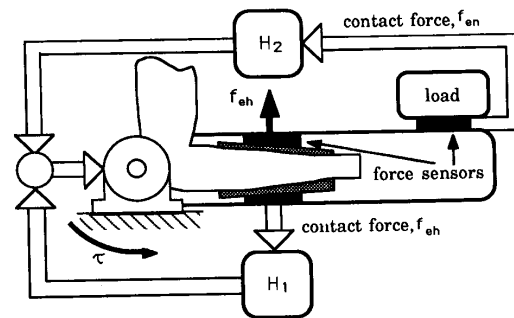


Figure 1: The schematic of the one-degree-of-freedom extender. f_{eh} and f_{en} are the forces imposed on the extender from the human and environment respectively.

The zero command for the primary controller results in zero speed for the extender. In other words, when there is no "push" from the human, the extender will be stationary. H_1 and H_2 are of paramount importance in the stability of the system of the human and the extender taken as a whole². For a given load, it is desirable to have the bandwidth of the extender wide so it can keep up with the high speed motion of the human arm. It is also desirable to have the contact force between the human and extender remain as small as possible so one can maneuver a large load with a small contact force³. It has been shown in Part I that, in order to achieve a fast response and a small (but nonzero) contact force, one needs large values for H_1 . However, one cannot choose an arbitrarily large value for H_1 ; the stability of the system must also be guaranteed. Here, it is explained how instability may occur in the system when a large value for H_1 is chosen. Suppose compensator H_1 has a large gain⁴ over a frequency range of operation. If the human decides to move up the object, the extender will move up with such a large velocity that it pulls the human arm up. This

² Similar analysis is given in references 12 and 13 to describe the stability of an *autonomous* robot interacting with an environment.

³ The contact force should be small but non-zero. It is necessary to have non-zero contact force so that the human always feels a constant portion of the actual load.

⁴ One can use the singular value for linear systems or L_∞ norm for nonlinear systems to represent the gain [26].

reverses the direction of the contact force between the human and the extender (downward in Figure 1). Then, the extender responds to the downward force with a large velocity which will pull down the human arm. This periodic motion occurs in a very short amount of time and the motion of the extender will become oscillatory and unbounded. H_1 must be designed such that its gain is large enough for the human to maneuver an object with high speed while stability is guaranteed. The trade-off between the performance and stability has been described in Part I and will experimentally be demonstrated here.

Sections 2, 3 and 4 describe the dynamic behavior of the extender, environment, and human arm while section 5 is dedicated to stability verification. In section 6, the performance of the system is analyzed where we show the amplification of the human power in the prototype extender.

2. Extender Dynamic Analysis

A single degree of freedom extender, shown in Figure 2, is used to experimentally verify the theoretical results on the extender stability and performance. This experimental extender consists of an outer tube (39.5 lbf) and an inner tube. The human arm, wrapped in a cylinder of rubber for a snug fit, is located in the inner tube. A piezoelectric load cell is placed between these tubes to measure the interaction force between the human arm and the extender, f_{eh} . A rotary hydraulic actuator (EXCELLO SS-8-100), which is mounted on a solid platform, is used to power the outer tube of the extender. The actuator shaft supported by two bearings is connected to the outer tube to transfer the power. In addition to the piezoelectric load cell, other sensing devices include a tachometer and an encoder (with a corresponding counter) to measure the angular speed and position of the motor shaft. An IBM/AT computer is used for data acquisition and control. Based on the information from these sensors, a control algorithm calculates a command signal to send to the servo controller board via a digital to analog (D/A) converter. The servo controller board outputs a current proportional to the command voltage resulting in a displacement of the servovalve spool.

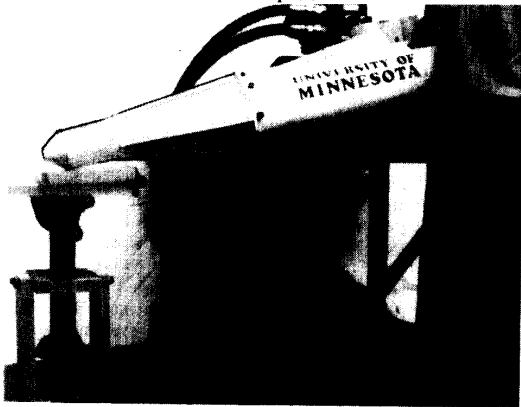


Figure 2: The experimental prototype extender pushing a spring and damper.

Figure 3 shows a velocity controller as the primary stabilizing controller for the extender. A PD controller is used to develop the closed loop velocity controller, $G_v(s)$, from u_e (digital number in the computer) to the extender velocity, v_e . Since $G_e(s)$ in Part I is defined as a mapping from u_e to the extender position, y_e , then $G_e(s) = G_v(s)/s$. u_p represents the command voltage to the servo controller board to produce the

output current, i . $G_p(s)$ and $G_d(s)$ are the transfer functions of the open loop extender that show how the extender responds to the input current, i , and the external forces, f_{en} (or f_{eh}), respectively. The extender velocity is measured for feedback via a tachometer with gain of K_t . The moment arm representing the effect of the human force, l_{eh} , is about one third of l_{en} . Figure 4a in Part I shows the schematic of the prototype extender where $l_{eh} = 1'$ and $l_{en} = 3'$.

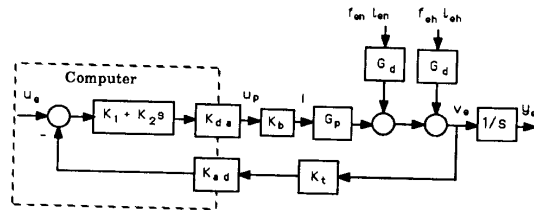


Figure 3: Block Diagram of the Closed Loop Velocity Controller, Tachometer gain: $K_t = 0.169$ volts/(rad/sec), Servo controller board gain: $K_b = 0.0077$ ampere/volt, Digital to Analog Converter: $K_{da} = 10$ volts/2048, Analog to Digital Converter: $K_{ad} = 2048/1.25$ volts

The theoretical and experimental derivations of G_p and G_d ⁵ have been given in Appendix A; equations 1 and 2 represent the resulting transfer functions for G_p and G_d .

$$G_p = \frac{v_e}{i} = \frac{533.7}{s^2 + \frac{s}{729} + 30.0} \quad (\text{rad/sec}/\text{Ampere}) \quad (1)$$

$$G_d = 139 \times 10^{-7} \frac{\frac{s}{24.2} + 1}{s^2 + \frac{s}{729} + 30.0} \quad (\text{rad/sec}/(\text{lbf} \cdot \text{inch})) \quad (2)$$

Using $K_1 = 0.01$ and $K_2 = 0.0004$, the theoretical value of the closed loop velocity control, G_v , can be calculated. The above values for K_1 and K_2 yield the widest bandwidth for G_v while the stability of the system is guaranteed in the presence of the unmodeled dynamics in the extender [10, 11]. Equation 3 represents the closed loop system where u_e is presented in rad and u_e is the digital number in the computer.

$$G_e = \frac{G_v}{s} = \frac{y_e}{u_e} = 0.00020 \frac{\frac{s}{25.0} + 1}{s^2 + \frac{s}{769.7} + 29.7} \frac{1}{s} \quad (3)$$

Although equation 3 represents a transfer function for the extender position, the extender is still under velocity control. Figure 4 shows the theoretical and experimental values for the bode plot of G_v . S_{en} is defined as the sensitivity of the extender position, y_e , in response to f_{en} , applied at a moment arm of $l_{en} = 3$ feet, while S_{eh} represents the analogous definition for the human force, f_{eh} , applied at a moment arm of $l_{eh} = 1'$. By inspection of the block diagram of Figure 3 and substituting the numerical values of the parameters, S_{en} can be found as follows:

⁵ Hereafter, the arguments for all transfer functions will be omitted.

$$S_{eh} = \frac{Y_e}{f_{en}} = 0.00047 \frac{\frac{s}{24.2} + 1}{\frac{s^2}{769.7} + \frac{s}{29.7} + 1} \frac{1}{s} \quad (\text{rad})/(\text{lbf}) \quad (4)$$

The theoretical steady state value of 0.00047 for S_{eh} can be compared with an experimental steady state value of 0.0005. Since the human arm force affects the extender about three times less than the environment force, S_{eh} is about three times less than S_{en} .

$$S_{eh} = \frac{l_{eh}}{l_{en}} S_{en} = 0.00016 \frac{\frac{s}{24.2} + 1}{\frac{s^2}{769.7} + \frac{s}{29.7} + 1} \frac{1}{s} \quad \text{rad/sec} \quad (5)$$

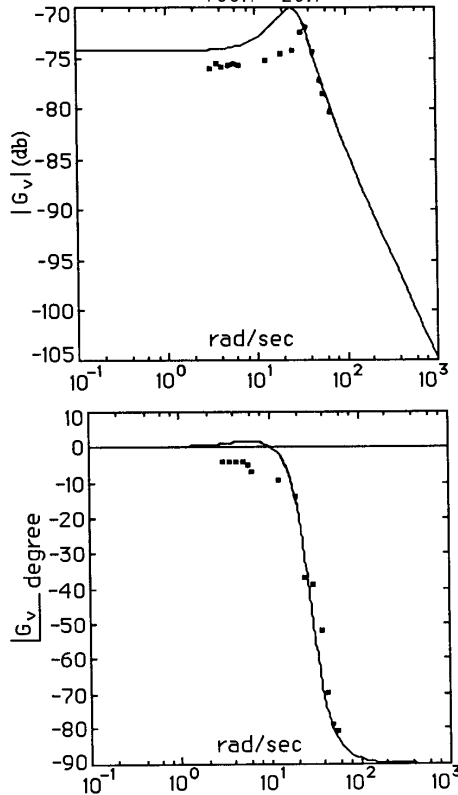


Figure 4: The Experimental and Theoretical Bode Plot of G_v . The primary stabilizing compensator has the bandwidth of about 10 rad/sec.

3. Environment Dynamic Analysis

E_n represents the environment dynamics. An automobile strut mounted on a custom fixture below the extender was used as an experimental environment (Figure 4a, Part I). This can be modeled as a linear spring and damper system, where inertial effects of the strut are neglected in comparison to the damping and spring effects. The environment stiffness and damping were measured experimentally to be 2100 lbf/rad and 200 lbf/(rad/sec), respectively. The units of radians refers to the angular displacement of the motor shaft. Expression 6 describes a

dynamic value for E_n , where the bandwidth of 10 rad/sec can be observed.

$$E_n = 200s + 2100 \quad \text{lbf/rad} \quad (6)$$

4. Human Arm Dynamic Analysis

The model derived here does not represent the complete sensitivity of the human arm, S_h , for all configurations; it only represents an approximate and experimentally verified model of the author elbow in the neighborhood of the configuration shown in Figure 2b. Since the extender is the only source of the external force, S_h is defined as a transfer function to map the extender position, Y_e , into the contact forces between the extender and human. The extender motion, Y_e , in the case of this prototype, is a rotating motion about the elbow joint. Assuming the human elbow behaves linearly in the neighborhood of the horizontal position, one can think of S_h as the human arm stiffness or, in the dynamic sense, as impedance. In order to arrive at this impedance, one may notice two impedances. The first impedance, denoted by I_{m1} , is associated with the flesh on the human elbow; this is passive, and the human has no control on it. The second impedance, I_{m2} , represents the impedance associated with the muscle forces; this is active and can be modulated by human thoughts via stiffening and loosening the muscles. The equivalent impedance of the human arm is equal to the serial addition of these impedances:

$$\frac{1}{S_h} = \frac{1}{I_{m1}} + \frac{1}{I_{m2}} \quad (7)$$

With this consideration, I_{m1} and I_{m2} are measured experimentally. The human flesh dynamics, I_{m1} , varies from human to human, as well as within the same human. The d.c. value of I_{m1} was experimentally derived by imposing loads on the elbow. This resulted in an approximate value for I_{m1} :

$$I_{m1} = 200 \text{ lbf/rad} \quad (8)$$

Several experiments were carried out to arrive at a model for I_{m2} . Various known loads were imposed on the elbow, and its response was measured when moving from horizontal level. The structure of I_{m2} was estimated as a second order impedance, $(\gamma s^2 + \phi s)$ assuming that the human arm motion has inertial and damping terms, but no spring term. The assumption of the zero spring term for this model initiated from the experimental observations; loading a heavy mass on a horizontally positioned human elbow moves the elbow continuously toward down without storing any energy in the elbow. Based on several experiments, the best educated estimation for the author's hand sensitivity prescribes $\gamma = 0.36$ lbf/(rad/sec²) and $\phi = 1.5$ lbf/(rad/sec). This suggests:

$$\frac{1}{S_h} = \frac{1}{200} + \frac{1}{0.36s^2 + 1.5s} \quad \text{rad/lbf} \quad (9)$$

5. Stability Analysis

A first order filter was chosen for H_1 to meet the design specification of equation 15 in Part I while $H_2 = 0$. Since E_n is a first order impedance (equation 6), H_1 must be chosen as a first order transfer function so that a constant proportion between f_{eh} and f_{en} can be achieved.

$$H_1 = \frac{K_h K_r K_{ad}}{\tau_o s + 1} \quad (10)$$

We choose $\tau_o = 0.1$ so the bandwidth of H_1 becomes the same as of E_n . K_h is the design parameter and must be chosen to

guarantee the stability and performance. Using K_r and K_{ad} , the force sensor and the A/D convertor gains (0.002 volts/lbf and 2048/1.25 volts) respectively), the numerical value for the compensator is given by equation 11.

$$H_1 = \frac{3.3 K_h}{\frac{s}{10} + 1} \quad (11)$$

It was shown that when $H_2 = 0$, the unconstrained system has a more strict stability bound on the compensator, H_1 , in comparison to the constrained system. Figure 5 shows the bound on H_1 for constrained and unconstrained maneuvers (inequalities 42 and 43 given in Part I). By inspection of Figure 5, it is clear that any H_1 that satisfies the unconstrained stability criterion will also satisfy the constrained stability condition. Since the extender usually consists of both constrained and unconstrained maneuvers, inequality 43 of Part I (unconstrained stability condition) is used as the stability condition for the prototype in the remainder of the analysis. This sufficient condition for stability is repeated here:

$$|H_1| < \frac{1}{|G_e|} \left| S_{eh} + \frac{1}{S_h} \right| \text{ for all } \omega \in (0, \infty) \quad (12)$$

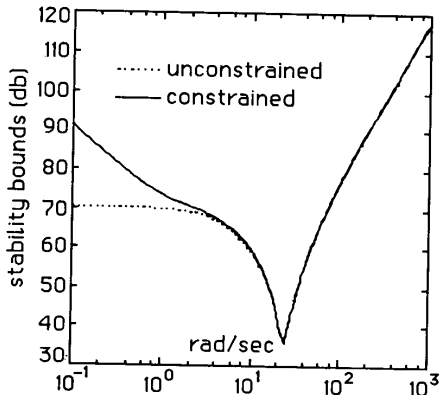


Figure 5: Stability Bounds of the Constrained and Unconstrained Systems; right hand sides of inequalities 42 and 43 in Part I.

The designer must choose a value for the gain of the compensator, K_h , to satisfy inequality 12 in order to ensure stability. Figure 6 shows the magnitude plot of the stability bound (right hand side of inequality 12) and compensator, H_1 , (left hand side of inequality 12) as a function of frequency, when the compensator gain, $K_h = 18$. In order to guarantee the stability of the system, K_h must be chosen to be smaller than 18 for all frequencies; however, if K_h is chosen to be larger than 18, then inequality 12 will be violated at some frequencies, and no conclusion about stability can be made. If the system were to be physically unstable, then it could be concluded that K_h must have been chosen to be larger than 18, violating inequality 12. Figures 7 and 8 show plots of f_{eh} and v_e , where $K_h = 15$. Since the stability condition (inequality 12) is satisfied for $K_h = 15$, the system will remain stable. If $K_h = 60$, the system exhibited instability as seen in Figures 9 and 10. This instability is present in the system in terms of oscillations. The plot of Figure 6 shows that the instability condition will be violated if $|H_1|$ is drawn with $K_h = 60$.

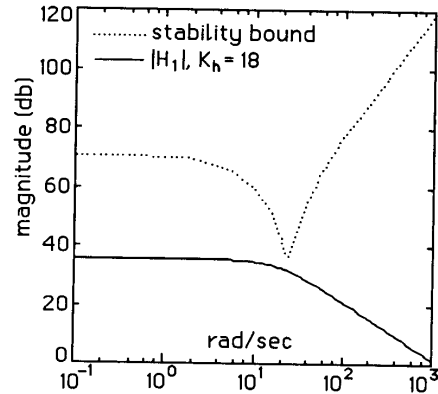


Figure 6: Stability condition of the unconstrained system (inequality 12) has been satisfied.

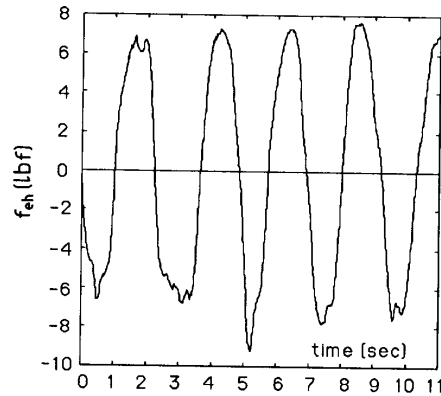


Figure 7: Stable Contact Force for $K_h = 15$; H_1 satisfies inequality 12.

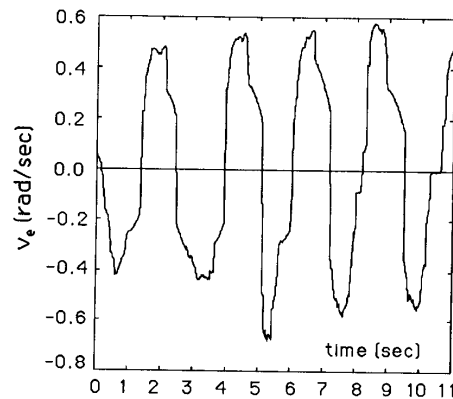


Figure 8: Stable Extender Velocity for $K_h = 15$; H_1 satisfies inequality 12.

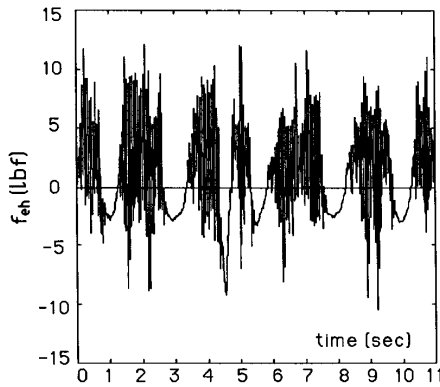


Figure 9: Unstable Contact Force for $K_h = 60$; H_1 violates inequality 12.

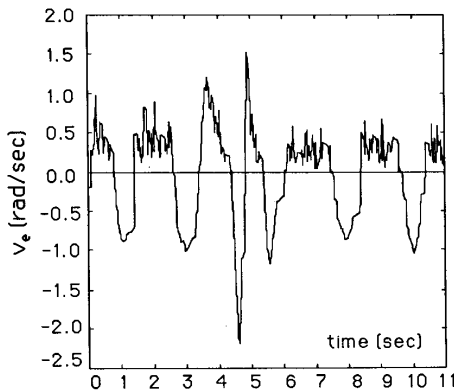


Figure 10: Unstable Extender Velocity for $K_h = 60$; H_1 violates inequality 12.

The root locus method was used to give the exact stability condition in this particular linear case. This is done to verify the conservative nature of the stability condition given by inequality 12. The inspection of block diagram of Figure 7 in Part I results in the following characteristic

$$1 + \frac{G_e H_1 S_h}{1 + S_{eh} S_h} = 0 \quad (13)$$

The root locus of the unconstrained system is shown in Figure 11 for various values of K_h . The root locus crosses the $j\omega$ axis when $K_h = 40$, resulting in the unstable system.

The stability condition expressed by inequality 12 is a sufficient condition only, and it cannot predict instability. Examining inequality 12 (depicted in Figure 6) leads to a smaller value for K_h to guarantee the stability than the one offered by root locus. Although the stability condition expressed by inequality 12 leads to a more conservative condition ($K_h = 18$), it does not depend on the internal structure of the extender and human arm model; it only requires the size of the mappings. The instability for the prototype was experimentally found to begin when the compensator gain, K_h , reached 30. This is in disagreement with the results of the root

locus stability analysis which predicted that instability would occur at $K_h = 40$ for the unconstrained system. The likely cause for this disagreement is due to the inaccurate modeling of the human arm dynamics, E , and the human sensitivity transfer function, S_h . In fact, we believe there must be other modes in the system other than the ones modeled in the system; these modes will become unstable when the gain of H is increased.

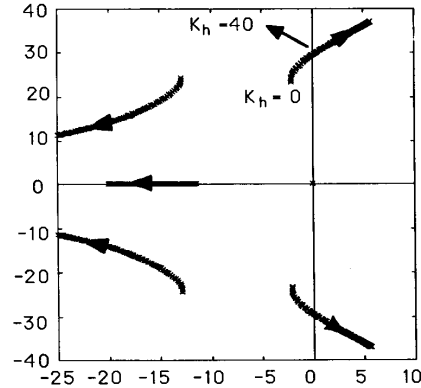


Figure 11: Root Locus of the Unconstrained System

6. Performance Analysis

The performance was studied under static and dynamic conditions. The static experiments show how the ratio of the interaction force between the extender and the environment and the interaction force between the human arm and the extender, $\left| \frac{f_{en}}{f_{eh}} \right|$, is a function of the compensator gain.

The dynamic experiments reinforce the results of the static experiments by showing the proportionality of the contact force

$$\left| \frac{f_{en}}{f_{eh}} \right| = \left| \frac{E_n S_{eh} + E_n G_e H_1}{1 + E_n S_{eh}} \right| \quad (14)$$

The prototype extender was tested under static conditions using compensator gains, K_h , ranging from 4 to 40 (constrained maneuvers allow for a larger stability range where K_h can be increased up to 40). At each compensator gain setting, the prototype was tested at 3 operating conditions: $f_{en} = 20$ lbf, $f_{en} = 40$ lbf, and $f_{en} = 50$ lbf. The parameters f_{eh} and f_{en} were measured with load cells, and an average steady state value of $\left| \frac{f_{en}}{f_{eh}} \right|$ over the three operating conditions was taken.

The experimental results were compared to the theoretical predictions given by equation 14 in Figure 12. A linear regression analysis on the experimental data in Figure 12 results in a slope of 1.3. In close agreement with the experimental data, the slope of the theoretical prediction is constant with a slope of 1.33.

The conclusion for this experiment is that applications requiring large interaction forces, f_{en} , require large values of compensator gain, K_h . For instance at full supply pressure, the extender is capable of lifting the front end of a car (roughly 300 lbf). If this is done with a large value of K_h , the human will feel a force (equal to f_{eh} in magnitude) on his/her arm on the order of 10 lbf. This 10 lbf force is a desirable magnitude as it is well within the range of human strength. With experience using the extender, the human can use the force, f_{eh} , as

feedback to properly adjust his/her contact with the extender to manipulate the car. It should be noted that, in applications requiring a large compensator gain, there is a higher likelihood of instability.

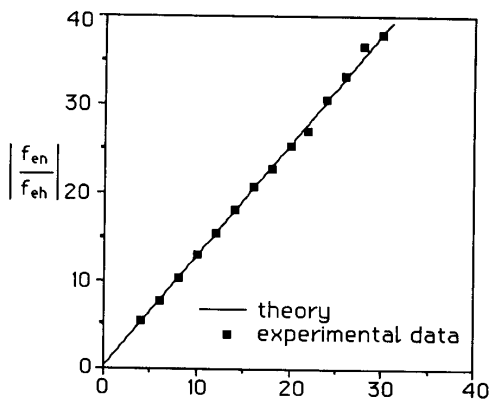


Figure 12: Static Experimental and Theoretical Plots of $\frac{|f_{en}|}{f_{eh}}$ vs K_h .

The dynamic experiments verify the transient characteristics of the theoretical transfer functions of the mappings relating to the extender and the environment. In equation 15, an expression for the interaction force between the extender and the environment, f_{en} , is derived by inspection of equation 7 in Part I.

$$f_{en} = -\frac{E_n S_{eh} + E_n G_o H_1}{1 + E_n S_{en}} f_{eh} \quad (15)$$

The basic procedure of the dynamic experiment consisted of using the prototype to push on the fabricated environment in a series of approximate step functions. The forces, f_{eh} and f_{en} , were measured and recorded in data files. The recorded f_{eh} was then used as an input to a computer simulation encompassing the dynamic behavior of the extender, human, and environment. Figures 13, 14, and 15 show the simulated and experimental value of f_{en} along with the recorded value of f_{eh} for two different maneuvers.

The experimental data and theoretical predictions were in close agreement. The first two plots were obtained using a low frequency human arm motion. This demonstrates the linearity between the input, f_{eh} , and the output, f_{en} . Note that the output force, f_{en} , is consistently twenty times larger than the input force, f_{eh} , at steady state regions. By inspection of the plots, it can be seen the more amplification is required, the larger H_1 must be chosen; however, large H_1 results in smaller stability range.

7. Summary and Conclusion

This paper presents concepts involving constrained motion of a class of human-controlled robotic manipulators called extenders. Extenders function to amplify the strength of the human operator, while utilizing the intelligence of the operator to spontaneously generate the command signal to the system. A single-degree-of-freedom extender has been built for theoretical and experimental verification of the dynamics and control involved in this hardware. The system performance has been defined as the amplification of the human power. It has been shown that the more amplification is required, the smaller the stability range of the system will be.

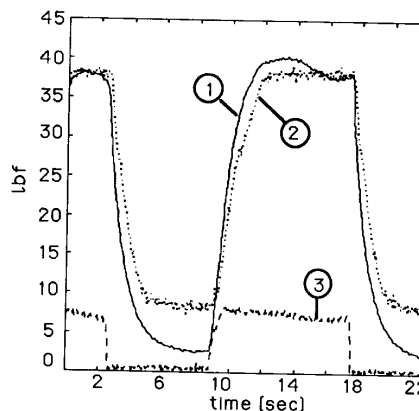


Figure 13: 1: simulated f_{en} , 2: experimental f_{en} , 3: $4 \times$ of the experimental f_{eh}

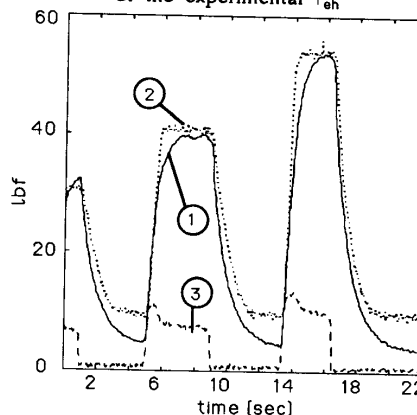


Figure 14: 1: simulated f_{en} , 2: experimental f_{en} , 3: $4 \times$ of the experimental f_{eh}

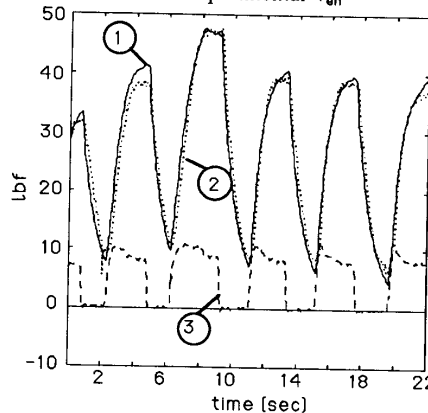


Figure 15: 1: simulated f_{en} , 2: experimental f_{en} , 3: $4 \times$ of the experimental f_{eh}

Appendix A

The experimental extender consists of an outer tube (39.5 lbf) and an inner tube (Figure 4a of Part I). The human arm, wrapped in a cylinder of rubber for a snug fit, is located in the inner tube. A piezoelectric load cell is placed between these tubes to measure the interaction force between the human arm and the extender, f_{eh} . A rotary hydraulic actuator (EXCELLO SS-8-100), which is mounted on a solid platform, is used to power the outer tube of the extender. The actuator shaft, supported by two bearings, is connected to the outer tube to transfer the power. The current, i , is the command input to the servovalve (MOOG 72-102-2) which allows the flow of hydraulic fluid to the rotary actuator. Since the extender will be used for constrained maneuvers, we model all external torques imposed on the extender by the product of external forces. f_{en} and f_{eh} represent the forces imposed on the environment from the human and from the environment, respectively (Figure A1).

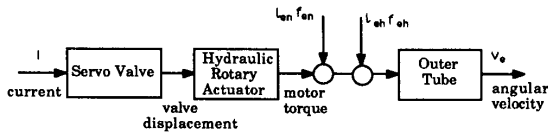


Figure A1: The Internal Block Diagram of G_p .

The dynamics of the hydraulic servovalve and rotary actuator system are described by equations A1, A2, and A3 [17]:

$$Q_1 = K_q i - K_p P_1 \quad (\text{valve equation}) \quad (A1)$$

$$Q_1 = v_e D_m + \frac{V_t}{4\beta_e} \frac{d}{dt} P_1 \quad (\text{flow continuity equation}) \quad (A2)$$

$$P_1 D_m = J \frac{d}{dt} v_e + f_{en} l_{en} + f_{eh} l_{eh} \quad (\text{Newton's Law}) \quad (A3)$$

where f_{en} , l_{en} , f_{eh} and l_{eh} are defined in Figure 4a of Part I and:

- Q_1 : load flow, in³/sec
- K_q : flow gain, (in³/sec)/amp
- i : current to drive servo valve, ampere
- K_p : pressure gain, in³/(sec lbf)
- P_1 : load pressure, psi
- v_e : angular velocity of the extender, rad/second
- D_m : actuator volumetric displacement, 7.62 in³/radian for EXCELLO SS-8-100
- J : outer tube moment of inertia, 38.8 in-lbf-sec²
- β_e : hydraulic fluid modulus of elasticity, 100,000psi
- V_t : total contained volume in actuator, 13.3 in³ for EXCELLO SS-8-100

Using equations A1, A2, and A3, a transfer function for the angular velocity of the open loop extender, v_e , is given by equation A4.

$$v_e = G_p i + G_d f_{en} l_{en} + G_d f_{eh} l_{eh} \quad (A4)$$

where:

$$G_p = \frac{K_q}{D_m} \frac{1}{s^2 + \frac{2\zeta_e s}{\omega_e} + 1}, \quad G_d = \frac{K_p}{D_m^2} \frac{V_t s + 1}{s^2 + \frac{2\zeta_e s}{\omega_e} + 1}$$

and $\omega_e = D_m \sqrt{\frac{4\beta_e}{V_t J}}$, $\zeta_e = \frac{K_p}{D_m} \sqrt{\frac{\beta_e J}{V_t}}$

The parameters of G_p were experimentally determined via the frequency response method up to 13.0 Hz (82 rad/sec).

The bode plot for G_p is given in Figure A2 where a second order transfer function (as defined above) was fit to the set of data. This results in:

$$\frac{K_q}{D_m} = 533.7 \text{ (rad/sec)/ampere,}$$

$$\omega_e = 27.0 \text{ rad/sec}$$

$$\zeta_e = 0.45$$

Using the above data, G_p is given in equation A5.

$$G_p = \frac{533.7}{s^2 + \frac{s}{30.0} + 1} \text{ (rad/sec)/ampere} \quad (A5)$$

By measuring the extender velocity in response to a constant load, the steady state value for G_d and, consequently, $\frac{K_p}{D_m^2}$ was determined to be 139×10^{-7} (rad/sec)/(lbf-inch). Using the values stated for V_t , β_e , and D_m , the numerical value for G_d is given by expression A6.

$$G_d = 139 \times 10^{-7} \frac{s}{\frac{s^2}{729} + \frac{s}{30.0} + 1} \text{ (rad/sec)/(lbf-inch)} \quad (A6)$$

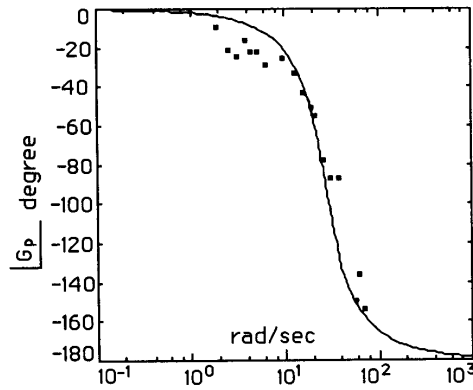
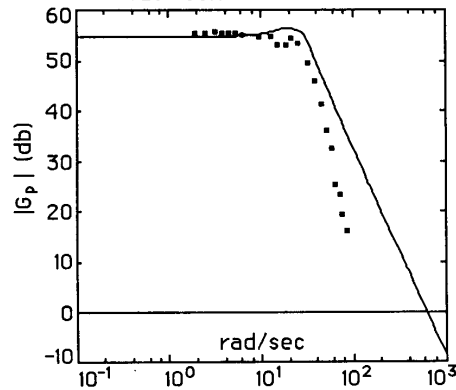


Figure A2: Experimental Data and Fitted G_p